

Comparative Evaluation of Despeckle Filtering In Ultrasound Imaging of the Carotid Artery

Christos P. Loizou, Constantinos S. Pattichis, *Senior Member, IEEE*, Christodoulos I. Christodoulou, Robert S. H. Istepanian, *Senior Member, IEEE*, Marios Pantziaris, and Andrew Nicolaides

Abstract—It is well-known that speckle is a multiplicative noise that degrades the visual evaluation in ultrasound imaging. The recent advancements in ultrasound instrumentation and portable ultrasound devices necessitate the need of more robust despeckling techniques for enhanced ultrasound medical imaging for both routine clinical practice and teleconsultation. The objective of this work was to carry out a comparative evaluation of despeckle filtering based on texture analysis, image quality evaluation metrics, and visual evaluation by medical experts in the assessment of 440 (220 asymptomatic and 220 symptomatic) ultrasound images of the carotid artery bifurcation. In this paper a total of 10 despeckle filters were evaluated based on local statistics, median filtering, pixel homogeneity, geometric filtering, homomorphic filtering, anisotropic diffusion, nonlinear coherence diffusion, and wavelet filtering. The results of this study suggest that the first order statistics filter *lsmv*, gave the best performance, followed by the geometric filter *gf4d*, and the homogeneous mask area filter *lsmisc*. These filters improved the class separation between the asymptomatic and the symptomatic classes based on the statistics of the extracted texture features, gave only a marginal improvement in the classification success rate, and improved the visual assessment carried out by the two experts. More specifically, filters *lsmv* or *gf4d* can be used for despeckling asymptomatic images in which the expert is interested mainly in the plaque composition and texture analysis; and filters *lsmv*, *gf4d*, or *lsmisc* can be used for the despeckling of symptomatic images in which the expert is interested in identifying the degree of stenosis and the plaque borders. The proper selection of a despeckle filter is very important in the enhancement of ultrasonic imaging of the carotid artery. Further work is needed to evaluate at a larger scale and in clinical practice the performance of the proposed despeckle filters in the automated segmentation, texture analysis, and classification of carotid ultrasound imaging.

I. INTRODUCTION

THE use of ultrasound in the diagnosis and assessment of arterial disease is well established because of its

Manuscript received January 8, 2005; accepted April 22, 2005.

C. P. Loizou is with the Department of Computer Science, Intercollege, CY-3507 Limassol, Cyprus (e-mail: christosl@lim.intercollege.ac.cy).

C. S. Pattichis is with the Department of Computer Science, University of Cyprus, Nicosia, Cyprus.

C. I. Christodoulou, M. Pantziaris, and A. Nicolaides are with the Cyprus Institute of Neurology and Genetics, Nicosia, Cyprus.

A. Nicolaides also is with the Department of Vascular Surgery, Imperial College London, UK.

R. S. H. Istepanian is with the Mobile Information and Network Technologies Research Center, School of Computing and Information Systems, Kingston University, Kingston-Upon-Thames, London, UK.

noninvasive nature, its low cost, and the continuing improvements in image quality [1]. Speckle, a form of locally correlated multiplicative noise corrupts medical ultrasound imaging making visual observation difficult [2], [3]. The presence of speckle noise in ultrasound images has been documented since the early 1970s when researchers such as Burckhardt [2], Wagner *et al.* [3], and Goodman [4] described the fundamentals and the statistical properties of the speckle noise. Speckle is not truly a noise in the typical engineering sense because its texture often carries useful information about the image being viewed. It is the primary factor that limits the contrast resolution in diagnostic ultrasound imaging, thereby limiting the detectability of small, low-contrast lesions and making the ultrasound images generally difficult for the nonspecialist to interpret [2], [3], [5], [6]. Due to the speckle presence, ultrasound experts with sufficient experience may not often draw useful conclusions from the images [6]. Speckle noise also limits the effective application of image processing and analysis algorithms (i.e., edge detection, segmentation) and display in two-dimensional (2-D) and volume rendering in 3-D. Therefore, speckle is most often considered a dominant source of noise in ultrasound imaging and should be filtered out [2], [5], [6] without affecting important features of the image. The objective of this paper was to carry out a comparative evaluation of despeckle filtering techniques based on texture analysis, image quality evaluation metrics, and visual assessment by experts on 440 ultrasound images of the carotid artery bifurcation. Preliminary results of this study were published in [7] and [8].

The wide spread of mobile and portable telemedicine ultrasound scanning instruments also necessitates the need for better image processing techniques in order to offer a clearer image to the medical practitioner. This makes the use of efficient despeckle filtering a very important task. Early attempts to suppress speckle noise were implemented by averaging of uncorrelated images of the same tissue recorded under different spatial positions [5], [9], [10]. Although these methods are effective for speckle reduction, they require multiple images of the same object to be obtained [11]. Speckle reducing filters originated from the synthetic aperture radar (SAR) community [9]. These filters have been applied to ultrasound imaging since the early 1980s [12]. Filters that are used widely in both SAR and ultrasound imaging include the Frost *et al.* [13], Lee [9], [14], [15], and Kuan *et al.* [11], [16].

Table I summarizes the despeckle filtering techniques that are investigated in this study, grouped under the

TABLE I
AN OVERVIEW OF DESPECKLE FILTERING TECHNIQUES.

| Speckle reduction technique | Investigator | Method | Filter name |
|-----------------------------|---------------------------------------|--|-------------|
| Local statistics | [7]–[14], [13]–[16] | Moving window using local statistics (a) mean (m), variance (σ^2). | lsmv |
| | [7]–[14] | (b) mean, variance, 3rd and 4th moments (higher moments) and entropy. | |
| | [32] | (c) Homogeneous mask area filters. | lsmisc |
| | [2]–[14], [15] | (e) Wiener filtering. | wiener |
| Median | [33] | Median filtering. | median |
| Homogeneity | [8] | Based on the most homogeneous neighborhood around each pixel. | homog |
| Geometric | [10] | Nonlinear iterative algorithm. | gf4d |
| Homomorphic | [2], [17], [18] | The image is logarithmically transformed, the FFT is calculated, denoised, the inverse FFT is calculated and exponentially transformed back. | homo |
| Anisotropic diffusion | [2], [5], [12], [13], [19], [20]–[23] | Nonlinear filtering technique for simultaneously performing contrast enhancement and noise reduction. Exponential damp kernel filters using diffusion. | ad |
| | [24] | Coherence enhancing diffusion. | nldif |
| Wavelet | [15], [25]–[29], [35] | Only the useful wavelet coefficients are used. | waveltc |

following categories: local statistics, median filtering, homogeneity, geometric, homomorphic, anisotropic diffusion, and wavelet filtering. Furthermore, in Table I the main investigators, the methodology used, and the corresponding filter names are given. These filters are briefly introduced in this section, and presented in greater detail in Section II.

Some of the local statistic filters are the Lee [9], [14], [15], the Frost *et al.* [13], and the Kuan *et al.* [11], [16]. The Lee and Kuan filters have the same structure, but the Kuan is a generalization of the Lee filter. Both filters form the output image by computing the central pixel intensity inside a filter-moving window, which is calculated from the average intensity values of the pixels and a coefficient of variation inside the moving window. Kuan *et al.* considered a multiplicative speckle model and designed a linear filter based on the minimum-mean-square error (MMSE) criterion that has optimal performance when the histogram of the image intensity is Gaussian distributed. The Lee [9] filter is a particular case of the Kuan filter based on a linear approximation made for the multiplicative noise model. The Frost *et al.* [13] makes a balance between the averaging and the all-pass filters. It was designed as an adaptive Wiener filter that assumed an autoregressive exponential model for the image.

In the homogeneity group, the filtering is based on the most homogeneous neighborhood around each image pixel [8]. Geometric filters [10] are based on nonlinear iterative

algorithms, which increment or decrement the pixel values in a neighborhood based upon their relative values. The method of homomorphic filtering [17], [18] is similar to the logarithmic point operations used in histogram improvement, in which dominant bright pixels are de-emphasized. In the homomorphic filtering, the fast Fourier transform (FFT) of the image is calculated, denoised, then the inverse FFT is calculated.

Some other despeckle filtering methods, such as anisotropic diffusion [2], [19], [20]–[23], speckle reducing anisotropic diffusion [5], and coherence anisotropic diffusion [24], presented recently in the literature, are nonlinear filtering techniques for simultaneously performing contrast enhancement and noise reduction by using the coefficient of variation [5]. Furthermore, in the wavelet category, filters for suppressing the speckle noise were documented. These filters are making use of a realistic distribution of the wavelet coefficients [2], [15], [25]–[30] in which only the useful wavelet coefficients are used. Different wavelet shrinkage approaches were investigated, usually based on Donoho's work [29].

The majority of speckle reduction techniques have certain limitations that can be briefly summarized as follows:

- They are sensitive to the size and shape of the window. The use of different window sizes greatly affects the quality of the processed images. If the window is too large, over smoothing will occur, subtle details of

the image will be lost in the filtering process, and edges will be blurred. However, a small window will decrease the smoothing capability of the filter and will not reduce speckle noise, thus making the filter not effective.

- Some of the despeckle methods based on window approaches require thresholds to be used in the filtering process, which have to be estimated empirically. The inappropriate choice of a threshold may lead to average filtering and noisy boundaries, thus leaving the sharp features unfiltered [7], [10], [14].
- Most of the existing despeckle filters do not enhance the edges, they only inhibit smoothing near the edges. When an edge is contained in the filtering window, the coefficient of variation will be high and smoothing will be inhibited. Therefore, speckle in the neighborhood of an edge will remain after filtering. They are not directional in the sense that, in the presence of an edge, all smoothing is precluded. Instead of inhibiting smoothing in directions perpendicular to the edge, smoothing in directions parallel to the edge is allowed.
- Different evaluation criteria for evaluating the performance of despeckle filtering are used by different studies. Although most of the studies use quantitative criteria such as the mean-square error (MSE) and speckle index (C), there are additional quantitative criteria such as texture analysis and classification, image quality evaluation metrics, and visual assessment by experts that could be investigated.

To the best of our knowledge, there is only one study that investigated despeckle filtering on ultrasound images of the carotid artery and proposed speckle reducing anisotropic diffusion as the most appropriate method [5]. This technique was compared with the Frost *et al.* [13], Lee [14], and the homomorphic filtering [18] and documented that anisotropic diffusion performed better.

In this study, we compare the performance of 10 despeckle filters on 440 ultrasound images of the carotid artery bifurcation. The performance of these filters was evaluated using texture analysis, the k-nearest neighbor (kNN) classifier, image quality evaluation metrics, and visual evaluation by two experts. The results of our study show that despeckle filtering improves the class separation between asymptomatic and symptomatic ultrasound images of the carotid artery.

In the following section, a brief overview of despeckle filtering techniques is presented. In Section III the methodology is presented, covering the material, recording of ultrasound images, texture and statistical analysis, the kNN classifier, image quality evaluation metrics, and the experiment carried out for visual evaluation are described. Sections IV and V present the results, and discussion, respectively.

II. DESPECKLE FILTERING

In order to be able to derive an efficient despeckle filter, a speckle noise model is needed. The speckle noise model may be approximated as multiplicative, if the envelope

signal received at the output of the beamformer of the ultrasound imaging system is captured before logarithmic compression and may be defined as:

$$y_{i,j} = x_{i,j}n_{i,j} + a_{i,j}, \quad (1)$$

where $y_{i,j}$ represents the noisy pixel in the middle of the moving window, $x_{i,j}$ represents the noise-free pixel, $n_{i,j}$ and $a_{i,j}$ represent the multiplicative and additive noise, respectively, and i, j are the indices of the spatial locations that belong in the 2-D space of real numbers, $i, j \in \mathbb{R}^2$. Logarithmic compression is applied to the envelope-detected echo signal in order to fit it in the display range [24], [31]. It has been shown that the logarithmic compression affects the speckle noise statistics in such a way that the local mean becomes proportional to the local variance rather than the standard deviation [24], [26], [28], [31] [see also (8)]. More specifically, logarithmic compression affects the high-intensity tail of the Rayleigh and Rician probability density function (PDF) more than the low-intensity part. As a result, the speckle noise becomes very close to white Gaussian noise corresponding to the uncompressed Rayleigh signal [31]. Because the effect of additive noise is considerably smaller compared with that of multiplicative noise, (1) may be written as:

$$y_{i,j} \approx x_{i,j}n_{i,j}. \quad (2)$$

Thus the logarithmic compression transforms the model in (2) into the classical signal in additive noise form as:

$$\log(y_{i,j}) = \log(x_{i,j}) + \log(n_{i,j}), \quad (3a)$$

$$g_{i,j} = f_{i,j} + nl_{i,j}. \quad (3b)$$

For the rest of the paper, the term $\log(y_{i,j})$, which is the observed pixel on the ultrasound image display after logarithmic compression, is denoted as $g_{i,j}$, and the terms $\log(x_{i,j})$, $\log(n_{i,j})$ which are the noise-free pixel and noise component after logarithmic compression, as $f_{i,j}$ and $nl_{i,j}$, respectively [see (3b)].

A. Local Statistics Filtering

Most of the techniques for speckle reduction filtering in the literature use local statistics. Their working principle may be described by a weighted average calculation using subregion statistics to estimate statistical measures over different pixel windows varying from 3×3 up to 15×15 . All these techniques assume that the speckle noise model has a multiplicative form as given in (2) [7]–[15], [24], [26].

1. *First Order Statistics Filtering (lsmv, wiener)*: The filters using the first order statistics such as the variance and the mean of the neighborhood may be described with the model as in (3). Hence, the algorithms in this class may be traced back to the following equation [5], [7]–[16]:

$$f_{i,j} = \bar{g} + k_{i,j}(g_{i,j} - \bar{g}), \quad (4)$$

where $f_{i,j}$ is the estimated noise-free pixel value, $g_{i,j}$ is the noisy pixel value in the moving window, \bar{g} is the local

mean value of an $N_1 \times N_2$ region surrounding and including pixel $g_{i,j}$, $k_{i,j}$ is a weighting factor with $k \in [0..1]$, and i, j , are the pixel coordinates. The factor $k_{i,j}$ is a function of the local statistics in a moving window. It can be found in the literature [9], [11], [14] and may be derived in different forms that:

$$k_{i,j} = (1 - \bar{g}^2 \sigma^2) / (\sigma^2 (1 + \sigma_n^2)), \quad (5)$$

$$k_{i,j} = \sigma^2 / (\bar{g}^2 \sigma_n^2 + \sigma^2), \quad (6)$$

$$k_{i,j} = (\sigma^2 - \sigma_n^2) / \sigma^2. \quad (7)$$

The values σ^2 and σ_n^2 represent the variance in the moving window and the variance of noise in the whole image, respectively. The noise variance may be calculated for the logarithmically compressed image by computing the average noise variance over a number of windows with dimensions considerably larger than the filtering window. In each window the noise variance is computed as:

$$\sigma_n^2 = \sum_{i=1}^p \sigma_p^2 / \bar{g}_p, \quad (8)$$

where σ_p^2 and \bar{g}_p are the variance and mean of the noise in the selected windows, respectively, and p is the index covering all windows in the whole image [24], [25], [31]. If the value of $k_{i,j}$ is 1 (in edge areas) this will result to an unchanged pixel, and a value of 0 (in uniform areas) replaces the actual pixel by the local average, \bar{g} , over a small region of interest [see (4)]. In this study the filter lsmv uses (5). The filter wiener uses a pixel-wise adaptive Wiener method [2]–[6], [13] implemented as given in (4), with the weighting factor $k_{i,j}$, as given in (7). For both despeckle filters lsmv and wiener the moving window size was 5×5 .

2. Homogeneous Mask Area Filtering: The lsmisc is a 2-D filter operating in a 5×5 pixel neighborhood by searching for the most homogenous neighborhood area around each pixel, using a 3×3 subset window [32]. The middle pixel of the 5×5 neighborhood is substituted with the average gray level of the 3×3 mask with the smallest speckle index, C , where C for log-compressed images is given by:

$$C = \sigma_s^2 / \bar{g}_s, \quad (9)$$

where σ_s^2 and \bar{g}_s represents the variance and mean of the 3×3 window. The window with the smallest C is the most homogenous semiwindow, which presumably does not contain any edge. The filter is applied iteratively until the gray levels of almost all pixels in the image do not change.

B. Median Filtering

The filter median [33] is a simple nonlinear operator that replaces the middle pixel in the window with the median-value of its neighbors. The moving window for the median filter was 7×7 .

C. Maximum Homogeneity Over a Pixel Neighborhood Filtering

The homog filter is based on an estimation of the most homogeneous neighborhood around each image pixel [34]. The filter takes into consideration only pixels that belong in the processed neighborhood (7×7 pixels) using (10), under the assumption that the observed area is homogeneous. The output image then is given by:

$$f_{i,j} = (c_{i,j} g_{i,j}) / \sum_{i,j} c_{i,j}, \text{ with}$$

$$c_{i,j} = 1 \text{ if } (1 - 2\sigma_n) \bar{g} \leq g_{i,j} \leq (1 + 2\sigma_n) \bar{g} \quad (10)$$

$$c_{i,j} = 0 \text{ otherwise.}$$

The homog filter does not require any parameters or thresholds to be tuned, thus making the filter suitable for automatic interpretation.

D. Geometric Filtering

The concept of the geometric filtering is that speckle appears in the image as narrow walls and valleys. The geometric filter, through iterative repetition, gradually tears down the narrow walls (bright edges) and fills up the narrow valleys (dark edges), thus smearing the weak edges that need to be preserved.

The gf4d filter [10] investigated in this study uses a nonlinear noise reduction technique. It compares the intensity of the central pixel in a 3×3 neighborhood with those of its eight neighbors and, based upon the neighborhood pixel intensities, it increments or decrements the intensity of the central pixel such that it becomes more representative of its surroundings. The operation of the geometric filter gf4d may be described with Fig. 1 and has the following form:

1. Select Direction and Assign Pixel Values: Select the direction north-south (NTST) and the corresponding three consecutive pixels a, b, c [see Fig. 1(a) and (b), respectively].

2. Carry Out Central Pixel Adjustments: Do the following intensity adjustments [see Fig. 1(b)]:

- if $a \geq b + 2$ then $b = b + 1$,
- if $a > b$ and $b \leq c$ then $b = b + 1$,
- if $c > b$ and $b \leq a$ then $b = b + 1$,
- if $c \geq b + 2$ then $b = b + 1$,
- if $a \leq b - 2$ then $b = b - 1$,
- if $a < b$ and $b \geq c$ then $b = b - 1$,
- if $c < b$ and $b \geq a$ then $b = b - 1$,
- if $c \leq b - 2$ then $b = b - 1$.

3. Repeat: Repeat steps 1 and 2 for west-east (WE) direction, west-north to south-east (WNT-STE) direction, and north-east to west-south direction (NTE to WST) [see Fig. 1(a)].

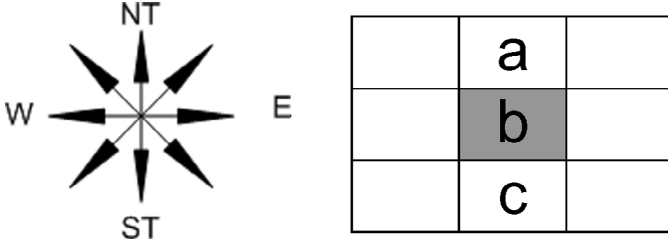


Fig. 1. (a) Directions of implementation of the gf4d geometric filter. (b) Pixels selected for the NTST direction (intensity of central pixel b is adjusted based on the values of intensities of pixels a , b , and c).

E. Homomorphic Filtering

The homo filter performs homomorphic filtering for image enhancement by calculating the FFT of the logarithmic compressed image, applying a denoising homomorphic filter function $H(\cdot)$, then performing the inverse FFT of the image [17], [18]. The homomorphic filter function $H(\cdot)$, may be constructed either using a band-pass Butterworth or a high-boost Butterworth filter. In this study, a high-boost Butterworth filter was used with the homomorphic function [17]:

$$H_{u,v} = \gamma_L + \frac{\gamma_H}{1 + (D_0/D_{u,v})^2}, \quad (11a)$$

with:

$$D_{u,v} = \sqrt{(u - N/2)^2 + (v - N/2)^2}, \quad (11b)$$

where $D_0 = 1.8$ is the cut of frequency of the filter, and $\gamma_L = 0.4$ and $\gamma_H = 0.6$ are the gains for the low and high frequencies, respectively, u and v are the spatial coordinates of the frequency transformed image, and N is the dimensions of the image in the u and v space.

This form of filtering sharpens features and flattens speckle variations in an image.

F. Diffusion Filtering

Diffusion filters remove noise from an image by modifying the image via solving a partial differential equation (PDE). The smoothing is carried out, depending on the image edges and their directions. Anisotropic diffusion is an efficient, nonlinear technique for simultaneously performing contrast enhancement and noise reduction. It smoothes homogeneous image regions but retains image edges [5], [22], [23] without requiring any information from the image power spectrum. Thus, it may be applied directly to logarithmic-compressed images. Consider applying the isotropic diffusion equation given by $dg_{i,j,t}/dt = \text{div}(d\nabla g)$ using the original noisy image $g_{i,j,t=0}$ as the initial condition, where $g_{i,j,t=0}$ is an image in the continuous domain, i, j specifies spatial position, t is an artificial time parameter, d is the diffusion constant, and ∇g is the image gradient. Modifying the image according to this linear

isotropic diffusion equation is equivalent to filtering the image with a Gaussian filter. In this section we will present conventional anisotropic diffusion (ad) and coherent nonlinear anisotropic diffusion (nldif).

1. *Anisotropic Diffusion Filtering:* Perona and Malik [23] replaced the classical isotropic diffusion equation, as described above, by the introduction of a function, $d_{i,j,t} = f(|\nabla g|)$, that smoothes the original image while trying to preserve brightness discontinuities with:

$$\begin{aligned} \frac{dg_{i,j,t}}{dt} &= \text{div}[d_{i,j,t}\nabla g_{i,j,t}] \\ &= \left[\frac{d}{di}d_{i,j,t} \frac{d}{di}g_{i,j,t} \right] + \left[\frac{d}{dj}d_{i,j,t} \frac{d}{dj}g_{i,j,t} \right], \quad (12a) \end{aligned}$$

where $|\nabla g|$ is the gradient magnitude, and $d(|\nabla g|)$ is an edge-stopping function that is chosen to satisfy $d \rightarrow 0$ when $|\nabla g| \rightarrow \infty$ so that the diffusion is stopped across edges. This function, called the diffusion coefficient, $d(|\nabla g|)$, which is a monotonically decreasing function of the gradient magnitude, $|\nabla g|$, yields intraregion smoothing not interregion smoothing [19], [20], [22], [23] by impeding diffusion at image edges. It increases smoothing parallel to the edge and stops smoothing perpendicular to the edge, as the highest gradient values are perpendicular to the edge and dilated across edges. The choice of $d(|\nabla g|)$ greatly can affect the extent to which discontinuities are preserved. For example if $d(|\nabla g|)$ is constant at all locations, then smoothing progresses in an isotropic manner. If $d(|\nabla g|)$ is allowed to vary according to the local image gradient, then we have anisotropic diffusion. A basic anisotropic PDE is given in (12a). Two different diffusion coefficients were proposed in [23] and also derived in [22]. The diffusion coefficient suggested were:

$$d(|\nabla g|) = \frac{1}{1 + (|\nabla g_{i,j}|/K)^2}, \quad (12b)$$

where K , in (12b) is a positive gradient threshold parameter, known as diffusion or flow constant [22]. In our study the diffusion coefficient in (12b) was used as it was found to perform better in our images of carotid artery.

A discrete formulation of the anisotropic diffusion in (12a) is [2], [22], [23]:

$$\begin{aligned} \frac{dg_{i,j}}{dt} &= \frac{\lambda}{|\eta_s|} \left\{ d_{i+1,j,t} [g_{i+1,j} - g_{i,j}] \right. \\ &\quad + d_{i-1,j,t} [g_{i-1,j} - g_{i,j}] + d_{i,j+1,t} [g_{i,j+1} - g_{i,j}] \\ &\quad \left. + d_{i,j-1,t} [g_{i,j-1} - g_{i,j}] \right\}, \quad (13a) \end{aligned}$$

where the new pixel gray value, $f_{i,j}$, at location i, j , is:

$$f_{i,j} = g_{i,j} + \frac{1}{4} \frac{dg_{i,j}}{dt}, \quad (13b)$$

where $d_{i+1,j,t}$, $d_{i-1,j,t}$, $d_{i,j+1,t}$, and $d_{i,j-1,t}$ are the diffusion coefficients for the west, east, north, and south pixel directions, in a four-pixel neighborhood, around the pixel

i, j , where diffusion is computed, respectively. The coefficient of variation leads to the largest diffusion in which the nearest-neighbor difference is largest (largest edge), and the smallest diffusion is calculated in which the nearest-neighbor difference is smallest (the weakest edge). The constant, $\lambda \in \mathbb{R}^+$, is a scalar that determines the rate of diffusion, η_s represents the spatial neighborhood of pixel, i, j , and $|\eta_s|$, is the number of neighbors (usually four, except at the image boundaries). Perona and Malik [23] linearly approximated the directional derivative in a particular direction as, $\nabla g_{i,j} = g_{i+1,j} - g_{i,j}$ (for the east direction of the central pixel i, j). Modifying the image according to the above in (13), which is a linear isotropic diffusion equation, is equivalent to filtering the image with a Gaussian filter. The parameters for the anisotropic diffusion filter used in this study were $\lambda = 0.25$, $\eta_s = 8$, and the parameter $K = 30$, which was used for the calculation of the edge-stopping function $d(|\nabla g|)$ in (12b).

2. Coherent Nonlinear Anisotropic Diffusion Filtering:

The applicability of the ad filter (12) is restricted to smoothing with edge enhancement, where $|\nabla g|$ has higher magnitude at edges. In general, the function $d(|\nabla g|)$ in (12) can be put into a tensor form that measures local coherence of structures such that the diffusion process becomes more directional in both the gradient and the contour directions, which represent the directions of maximum and minimum variations, respectively. Therefore, the nldif filter will take the form:

$$\frac{dg_{i,j,t}}{dt} = \text{div}[D\nabla g], \quad (14)$$

where $D \in \mathbb{R}^{2 \times 2}$ is a symmetric positive, semidefinite diffusion tensor representing the required diffusion in both gradient and contour directions and, hence, enhancing coherent structures as well as edges. The design of D , as well as the derivation of the coherent nonlinear anisotropic diffusion model, may be found in [24] and is given as:

$$D = (\omega_1 \ \omega_2) \begin{pmatrix} \lambda_1 & 0 \\ 0 & \lambda_2 \end{pmatrix} \begin{pmatrix} \omega_1^T \\ \omega_2^T \end{pmatrix}, \quad (15a)$$

with:

$$\lambda_1 = \begin{cases} \alpha \left(1 - \frac{(\mu_1 - \mu_2)^2}{s^2} \right) & \text{if } (\lambda_1 - \lambda_2)^2 \leq s^2 \\ 0, & \text{else} \end{cases}, \quad (15b)$$

$$\lambda_2 = \alpha,$$

where the eigenvectors ω_1, ω_2 and the eigenvalues λ_1, λ_2 correspond to the directions of maximum and minimum variations and the strength of these variations, respectively. The flow at each point is affected by the local coherence, which is measured by $(\mu_1 - \mu_2)$ in (15b).

The parameters used in this study for the nldif filter were $s^2 = 2$ and $\alpha = 0.9$, which were used for the

calculation of the diffusion tensor D , and the parameter step size $m = 0.2$, which defined the number of diffusion steps performed. The local coherence is close to zero in very noisy regions, and diffusion must become isotropic ($\mu_1 = \mu_2 = \alpha = 0.9$), and in regions with lower speckle noise the local coherence must correspond to $(\mu_1 - \mu_2)^2 > s^2$ [24].

G. Wavelet Filtering

Speckle reduction filtering in the wavelet domain, used in this study, is based on the idea of the Daubechies Symlet wavelet and on soft-thresholding denoising, first proposed by Donoho [29]. The method was also investigated by [25], [26], [35], [36]. The Symlets family of wavelets, although not perfectly symmetrical, were designed to have the least asymmetry and highest number of vanishing moments for a given compact support [29]. The wavelet filter, implemented in this study is described as follows:

- Estimate the variance of the speckle noise, σ_n^2 , from the logarithmic transformed noisy image with (8).
- Compute the discrete wavelet transform (DWT), using the Symlet wavelet for two scales.
- For each subband
 - Compute a threshold [27], [29]:

$$T = \begin{cases} (T_{\max} - \alpha(j-1)) \sigma_n & \text{if } T_{\max} - \alpha(j-1) \succ T_{\min} \\ T_{\min} \sigma_n, & \text{else} \end{cases} \quad (16)$$

where α is a decreasing factor between two consecutive levels, T_{\max} is a maximum factor for σ_n , and T_{\min} is a minimum factor. The threshold T is primarily calculated using σ_n and a decreasing factor, $T_{\max} - \alpha(j-1)$.

- Apply the thresholding procedure above on the wavelet coefficients.
- Invert the multiscale decomposition to reconstruct the despeckled image f .

III. METHODOLOGY

A. Material

A total of 440 ultrasound images of the carotid artery bifurcation (220 asymptomatic and 220 symptomatic) were investigated in this study. Asymptomatic images were recorded from patients at risk of atherosclerosis in the absence of clinical symptoms. Symptomatic images were recorded from patients at risk of atherosclerosis, who already have developed clinical symptoms, such as a stroke episode.

B. Recording of Ultrasound Images

In this study ultrasound images of the carotid artery bifurcation were acquired using the ATL HDI-3000 ul-

trasound scanner (ATL Ultrasound, Bothell, WA). The ATL HDI-3000 ultrasound scanner is equipped with 64 elements fine pitch high-resolution, 38-mm broadband array, a multielement ultrasound scan head with an operating frequency range of 4–7 MHz, an acoustic aperture of 10×8 mm, and a transmission focal range of 0.8–11 cm [37]. In this work all images were recorded as they are displayed in the ultrasound monitor after logarithmic compression. The images were recorded digitally on a magneto-optical drive, with a resolution of 768×756 pixels with 256 gray levels. The image resolution was 16.66 pixels/mm.

C. Despeckle Filtering

Ten despeckle filters were investigated as presented in Section II and were applied on the 440 logarithmically compressed ultrasound images.

D. Texture Analysis

Texture provides useful information for the characterization of atherosclerotic plaque [38]. In this study, a total of 56 different texture features were extracted both from the original and the despeckled images as follows [38], [39]:

1. *Statistical Features*: SF: Mean, median, variance (σ^2), skewness (σ^3) kurtosis (σ^4), and Speckle index (σ^2/m).

2. *Spatial Gray Level Dependence Matrices*: SGLDM as proposed by Haralick *et al.* [39]: angular second moment, contrast, correlation, sum of squares variance, inverse difference moment, sum average, sum variance, sum entropy, entropy, difference variance, difference entropy, information measures of correlation. Each feature was computed using a distance of one pixel. Also for each feature the mean values and the range of values were computed and were used as two different feature sets.

3. *Gray Level Difference Statistics*: GLDS [40]: contrast, angular second moment, entropy, and mean.

4. *Neighborhood Gray Tone Difference Matrix*: NGTDM [41]: coarseness, contrast, business, complexity, and strength.

5. *Statistical Feature Matrix*: SFM [42]: coarseness, contrast, periodicity, and roughness.

6. *Laws Texture Energy Measures*: TEM [42]: For the laws TEM extraction, vectors of length $l = 7$, $L = (1, 6, 15, 20, 15, 6, 1)$, $E = (-1, -4, -5, 0, 5, 4, 1)$ and $S = (-1, -2, 1, 4, 1 - 2, -1)$ were used, where L performs local averaging, E acts as an edge detector, and S acts as a spot detector. The following TEM features were extracted: LL-texture energy (TE) from LL kernel, EE-TE from EE kernel, SS-TE from SS kernel, LE-average TE from LE and EL kernels, ES-average TE from ES and SE kernels, and LS-average TE from LS and SL kernels.

7. *Fractal Dimension Texture Analysis*: FDTA [42]: Hurst coefficient, $H^{(k)}$, for resolutions $k = 1, 2, 3, 4$.

8. *Fourier Power Spectrum*: FPS [42]: radial sum and angular sum.

E. Distance Measures

In order to identify the most discriminant features separating asymptomatic and symptomatic ultrasound images before and after despeckle filtering, the following distance measure was computed for each feature [38]:

$$dis_{zc} = |m_{za} - m_{zs}| / \sqrt{\sigma_{za}^2 + \sigma_{zs}^2}, \quad (17)$$

where z is the feature index, c if o indicates the original image set and if f indicates the despeckled image set, m_{za} and m_{zs} are the mean values, and σ_{za} and σ_{zs} are the standard deviations of the asymptomatic and symptomatic classes, respectively. The most discriminant features are the ones with the highest distance values [38]. If the distance after despeckle filtering is increased, i.e.:

$$dis_{zf} > dis_{zo}, \quad (18)$$

then it can be derived that the classes may be better separated.

For each feature, a percentage distance was computed as:

$$feat_dis_z = (dis_{zf} - dis_{zo}) 100. \quad (19)$$

For each feature set, a score distance was computed as:

$$Score_Dis = (1/N) \sum_{z=1}^N (dis_{zf} - dis_{zo}) 100, \quad (20)$$

where N is the number of features in the feature set. It should be noted that, for all features, a larger feature distance shows improvement.

F. Univariate Statistical Analysis

The Wilcoxon rank sum test was used in order to detect if, for each texture feature, a significant (S) difference or not (N) exists between the original and the despeckled images at $p < 0.05$.

G. kNN Classifier

The statistical kNN classifier using the Euclidean distance with $k = 7$ also was used to classify a plaque image as asymptomatic or symptomatic [38]. The leave-one-out method was used for evaluating the performance of the classifier, in which each case is evaluated in relation to the rest of the cases. This procedure is characterized by no bias concerning the possible training and evaluation bootstrap sets. The kNN classifier was chosen because it is simple to implement and computationally very efficient. This is highly desired due to the many feature sets and filters tested [42].

H. Image Quality Evaluation Metrics

Differences between the original, $g_{i,j}$, and the despeckled, $f_{i,j}$, images were evaluated using image quality evaluation metrics. The following measures, which are easy to compute and have clear physical meaning, were computed. The MSE:

$$MSE = \frac{1}{MN} \sum_{i=1}^M \sum_{j=1}^N (g_{i,j} - f_{i,j})^2, \quad (21)$$

which measures the quality change between the original and processed image in an $M \times N$ window [43]. The root MSE (RMSE), which is the square root of the squared error averaged over an $M \times N$ window [44]:

$$RMSE = \sqrt{\frac{1}{MN} \sum_{i=1}^M \sum_{j=1}^N (g_{i,j} - f_{i,j})^2}. \quad (22)$$

The error summation in the form of the Minkowski metric, which is the norm of the dissimilarity between the original and the despeckled images [45]:

$$Err = \left(\frac{1}{MN} \sum_{i=1}^M \sum_{j=1}^N |g_{i,j} - f_{i,j}|^\beta \right)^{1/\beta}, \quad (23)$$

computed for $\beta = 3$ (Err_3) and $\beta = 4$ (Err_4). For $\beta = 2$, the RMSE is computed as in (22), whereas for $\beta = 1$ the absolute difference, and for $\beta = \infty$ the maximum difference measure.

The geometric average error (GAE) is computed as in [46]. The GAE is approaching zero, if there is a very good transformation (small differences) between the original and the despeckled image, and high vice versa. This measure also is used for teleultrasound, when transmitting ultrasound images and is defined as:

$$GAE = \left(\prod_{i=1}^M \prod_{j=1}^N \sqrt{g_{i,j} - f_{i,j}} \right)^{1/MN}. \quad (24)$$

The signal-to-noise ratio (SNR) is given by [47]:

$$SNR = 10 \log_{10} \frac{\sum_{i=1}^M \sum_{j=1}^N (g_{i,j}^2 + f_{i,j}^2)}{\sum_{i=1}^M \sum_{j=1}^N (g_{i,j} - f_{i,j})^2}. \quad (25)$$

The peak SNR (PSNR) is computed using [47]:

$$PSNR = -10 \log_{10} \frac{MSE}{g_{\max}^2}, \quad (26)$$

where g_{\max}^2 is the maximum intensity in the unfiltered image. The PSNR is higher for a better-transformed image and lower for a poorly transformed image. It measures

image fidelity, which is how closely the despeckled image resembles the original image.

The mathematically defined universal quality index [48] models any distortion as a combination of three different factors: loss of correlation, luminance distortion, and contrast distortion and is derived as:

$$Q = \frac{\sigma_{gf}}{\sigma_f \sigma_g} \cdot \frac{2\bar{f}\bar{g}}{(\bar{f})^2 + (\bar{g})^2} \cdot \frac{2\sigma_f \sigma_g}{\sigma_f^2 + \sigma_g^2}, \quad -1 < Q < 1, \quad (27)$$

where \bar{g} and \bar{f} represent the mean of the original and despeckled values with their standard deviations, σ_g and σ_f , of the original and despeckled values of the analysis window, and σ_{gf} represents the covariance between the original and despeckled windows. Q is computed for a sliding window of size 8×8 without overlapping. Its highest value is 1 if $g_{i,j} = f_{i,j}$; its lowest value is -1 if $f_{i,j} = 2\bar{g} - g_{i,j}$.

The structural similarity index between two images [45], which is a generalization of (27), is given by:

$$SSIN = \frac{(2\bar{g}\bar{f} + c_1)(2\sigma_{gf} + c_2)}{(\bar{g}^2 + \bar{f}^2 + c_1)(\sigma_g^2 + \sigma_f^2 + c_2)}, \quad -1 < SSIN < 1, \quad (28)$$

where $c_1 = 0.01dr$ and $c_2 = 0.03dr$, with $dr = 255$ representing the dynamic range of the ultrasound images. The range of values for the SSIN lies between -1 , for a bad and 1 for a good similarity between the original and despeckled images, respectively. It is computed, similarly to the Q measure, for a sliding window of size 8×8 without overlapping.

It is noted that a new image quality metric, based on natural scene statistics and mutual information between the original and the filtered images, has recently been proposed by Sheikh *et al.* [49]. This metric will be investigated in a future study.

I. Visual Evaluation by Experts

Visual evaluation can be broadly categorized as the ability of an expert to extract useful anatomical information from an ultrasound image. The visual evaluation varies, of course, from expert to expert and is subject to the observer's variability [50]. The visual evaluation in this study was carried out according to the International Telecommunication Union Radiocommunication Sector (ITU-R) recommendations with the double stimulus continuous quality scale (DSCQS) procedure [46]. A total of 100 ultrasound images of the carotid artery bifurcation (50 asymptomatic and 50 symptomatic) were evaluated visually by two vascular experts—a cardiovascular surgeon and a neurovascular specialist—before and after despeckle filtering. For each case, the original and the despeckled images (despeckled with filters lsmv, lsminsc, median, wiener, homog, gf4d, homo, ad, nldif, and waveltc) were presented without labelling at random to the two experts. The experts were asked to assign a score in the one-to-five scale corresponding to low and high subjective visual perception criteria.

Five was given to an image with the best visual perception. Therefore, the maximum score for a filter is 500, if the expert assigned the score of five for all 100 images. For each filter, the score was divided by five to be expressed in percentage format. The experts were allowed to give equal scores to more than one image in each case. For each class and for each filter, the average score was computed.

The two vascular experts evaluated the area around the distal common carotid, 2–3 cm before the bifurcation and the bifurcation. It is known that measurements taken from the far wall of the carotid artery are more accurate than those taken from the near wall [51]. Furthermore, the experts were examining the image in the lumen area to identify the existence of plaque or not.

IV. RESULTS

In this section we present the results of the 10 despeckle filters described in Section II, applied on 220 asymptomatic and 220 symptomatic ultrasound images of the carotid artery bifurcation. A total of 56 texture features were computed, and the most discriminant ones are presented. Furthermore, the performance of these filters is investigated for discriminating between asymptomatic and symptomatic images using the statistical kNN classifier. Moreover, nine different image quality evaluation metrics were computed, as well as visual evaluation scores carried out by two experts.

A. Evaluation of Despeckle Filtering on a Symptomatic Ultrasound Image

Fig. 2 shows an ultrasound image of the carotid together with the despeckled images. The best visual results as assessed by the two experts were obtained by the filters lsmv and lsminsc; the filters gf4d, ad, and nldif also showed good visual results but smoothed the image considerably and thus edges and subtle details may be lost. Filters that showed a blurring effect are the median, wiener, homog, and waveltc. Filters wiener, homog, and waveltc showed poorer visual results.

B. Texture Analysis: Distance Measures

Despeckle filtering and texture analysis were carried out on 440 ultrasound images of the carotid. Table II tabulates the results of $feat_dis_z$ (19), and $Score_Dis$ (20), for SF, SGLDM range of values and NGTDM feature sets for the 10 despeckle filters. Only the results of these feature sets are presented because they were the ones with the best performance. The filters are categorized in local statistics, median, maximum homogeneity (HF), geometric (GF), homomorphic (HM), diffusion and wavelet filters, as introduced in Sections I and II. Also, the number of iterations (Nr. of It.) for each filter is given, which was selected based on C and on the visual evaluation of the

two experts. When C was minimally changing, the filtering process was stopped. The bold numbers represent the values that showed an improvement after despeckle filtering compared to the original. The last row in each subtable shows the $Score_Dis$ for all features in which the highest value indicates the best filter in the subtable. Additionally, a total score distance $Score_Dis_T$ was computed for all feature sets shown in the last row of Table II. Some of the despeckle filters shown in Table II are changing a number of texture features by increasing the distance between the two classes (positive values in Table II) and, therefore, making the identification and separation between asymptomatic and symptomatic plaques more feasible. A positive feature distance shows improvement after despeckle filtering; a negative feature shows deterioration.

In the first part of Table II, the results of the SF features are presented in which the best $Score_Dis$ is given for the filter homo followed by the lsminsc, lsmv, homog, nldif, waveltc, median, and wiener, with the worst $Score_Dis$ given by gf4d. All filters reduced the speckle index, C . Almost all filters reduced significantly the variance, σ^2 , and the kurtosis, σ^3 , of the histogram, as may be seen from the bold numbers in the first part of Table II.

In the second part of Table II, the results of the SGLDM-range of values features set are tabulated. The filters with the highest $Score_Dis$ in the SGLDM range of values features set, are homo, lsminsc, median, ad, and homog; all other the filters (nldif, wiener, waveltc, gf4d, lsmv) are presenting a negative $Score_Dis$. Texture features, which improved in most of the filters, are the contrast, correlation, sum of squares variance, sum average, and sum variance.

In the third part of Table II, for the NGTDM feature set, almost all filters showed an improvement in $Score_Dis$. Best filters in the NGTDM feature set were the homo, lsminsc, homog, and lsmv. Texture features improved at most were the completion, coarseness, and contrast. The completion of the image was increased by all filters.

In the last row of Table II, the total score distance, $Score_Dis_T$, for all feature sets is shown; best values were obtained by the filters homo, lsminsc, median, lsmv, homog, and ad.

C. Texture Analysis: Univariate Statistical Analysis

Table III shows the results of the rank sum test, which was performed on the SGLDM range of values features set of Table II, for the 10 despeckle filters. The test was performed to check if significant differences exist between the features computed on the 440 original and the 440 despeckled images. Filters that resulted with the most significant number of features after despeckle filtering as shown with the score row of Table III were: lsmv, gf4d, lsminsc and nldif. The rest of the filters gave a lower number of significantly different features. Features that showed a significant difference after filtering were the inverse difference moment (IDM), angular second moment (ASM), sum of entropy,

TABLE II
FEATURE DISTANCE (18) AND SCORE_{DIS} (19) FOR SF, SGLDM RANGE OF VALUES, AND NGTDM TEXTURE FEATURE SETS BETWEEN ASYMPTOMATIC AND SYMPTOMATIC CAROTID PLAQUE ULTRASOUND IMAGES.¹

| Feature Nr. of It. | Local statistics | | | | HF | GF | HM | Diffusion | | Wavelet |
|--|------------------|------------|-----------|-----------|------------|----------|------------|------------|-----------|-----------|
| | lsmv | lsminsc | wiener | median | homog | gf4d | homo | ad | nldif | waveltc |
| | 4 | 1 | 2 | 2 | 1 | 3 | 2 | 20 | 5 | 5 |
| SF—Statistical features | | | | | | | | | | |
| Mean | 14 | 22 | 19 | 4 | 11 | 3 | 164 | 18 | 5 | 15 |
| Median | -5 | -17 | -26 | -5 | -5 | -15 | 110 | -29 | -6 | -15 |
| σ^2 | 18 | 38 | 18 | 7 | 13 | -2 | 140 | 9 | 7 | 18 |
| σ^3 | 12 | 16 | 5 | 9 | 7 | -0.1 | 149 | 17 | 7 | 8 |
| σ^4 | -12 | -14 | -7 | -6 | -4 | -3 | 117 | -21 | 6 | -9 |
| C | 0.4 | 0.3 | 0.3 | 0.4 | 0.3 | 0.4 | 0.08 | 0.3 | 0.4 | 0.3 |
| <i>Score_{dis}</i> | 27 | 45 | 9 | 9 | 22 | -17 | 680 | -6 | 19 | 17 |
| SGLDM range of values—Spatial gray level dependence matrix | | | | | | | | | | |
| ASM ² | -21 | -0.5 | -29 | 2 | -4 | -8 | -47 | -25 | -17 | -20 |
| Contrast | 47 | 107 | 14 | 64 | 32 | -3 | 165 | 104 | 13 | 22 |
| Correlation | 12 | 59 | 15 | 24 | -5 | 2 | 10 | 54 | -4 | -4 |
| SOSV | 9 | 40 | 18 | 10 | 16 | -2 | 101 | 9 | 8 | 20 |
| IDM | -50 | -11 | -48 | 2 | -29 | -8 | 94 | -54 | -34 | -43 |
| SAV | 17 | 24 | 23 | 7 | 15 | 3 | 169 | 22 | 6 | 18 |
| $\sum Var$ | 19 | 38 | 18 | 9 | 15 | -2 | 90 | 9 | 8 | 20 |
| $\sum Entr$ | -34 | -14 | -49 | 3 | -19 | -4 | -11 | -47 | -30 | -36 |
| <i>Score_{dis}</i> | -1 | 243 | -38 | 121 | 21 | -22 | 571 | 72 | -50 | -23 |
| NGTDM—Neighborhood gray tone difference matrix | | | | | | | | | | |
| Coarseness | 30 | 87 | 4 | 9 | -16 | -7 | 72 | -36 | -37 | -33 |
| Contrast | 7 | -0.3 | -9 | 8 | 0.4 | -4 | 105 | 5 | -27 | -15 |
| Busyness | 17 | 26 | -30 | 8 | 1 | -4 | 48 | -14 | -39 | 8 |
| Completion | 64 | 151 | 21 | 53 | 80 | 2 | 150 | 63 | 18 | 27 |
| <i>Score_{dis}</i> | 118 | 264 | -14 | 78 | 66 | -13 | 375 | 18 | -85 | -13 |
| <i>Score_{dis,T}</i> | 144 | 551 | -43 | 208 | 108 | -52 | 1626 | 84 | -116 | -19 |

¹Bold numbers show improvement after despeckle filter.

²ASM, angular 2nd moment; SOSV, sum of squares variance; IDM, inverse difference moment; SAV, sum average; $\sum Var$, sum variance; HF, homogeneity; GF, geometric; HM, homomorphic.

TABLE III
WILCOXON RANK SUM TEST FOR THE SGLDM RANGE OF VALUES TEXTURE FEATURES APPLIED ON THE 440 ULTRASOUND IMAGES OF CAROTID PLAQUE BEFORE AND AFTER DESPECKLE FILTERING. THE TEST SHOWS WITH S AND N, THE FEATURES THAT ARE AND ARE NOT SIGNIFICANTLY DIFFERENT AFTER FILTERING AT $P < 0.05$, RESPECTIVELY.

| Feature | Local statistics | | | Median | HF | GF | HM | Diffusion | | Wavelet | Score ² |
|------------------|------------------|---------|--------|--------|-------|------|------|-----------|-------|---------|--------------------|
| | lsmv | lsminsc | wiener | median | homog | gf4d | homo | ad | nldif | waveltc | |
| ASM ¹ | S | S | N | N | S | S | N | S | S | S | 7 |
| Contrast | S | N | N | N | N | S | N | N | S | N | 3 |
| Correlation | S | S | N | N | N | S | N | N | N | N | 3 |
| SOSV | S | N | N | N | N | S | N | N | N | N | 2 |
| IDM | S | S | N | S | S | S | S | N | S | S | 8 |
| SAV | N | N | N | N | N | N | N | N | N | N | 0 |
| $\sum Var$ | S | S | N | N | N | N | N | N | N | N | 2 |
| $\sum Entropy$ | S | S | N | N | N | S | N | N | S | S | 5 |
| Score | 7 | 5 | 0 | 1 | 2 | 6 | 1 | 1 | 4 | 3 | |

¹ASM, angular 2nd moment; SOSV, sum of squares variance; IDM, inverse difference moment; SAV, sum average; $\sum Var$, sum variance; HM, homomorphic; HF, homogeneity; GF, geometric; HM, homomorphic.

²Score, illustrates the number of S.

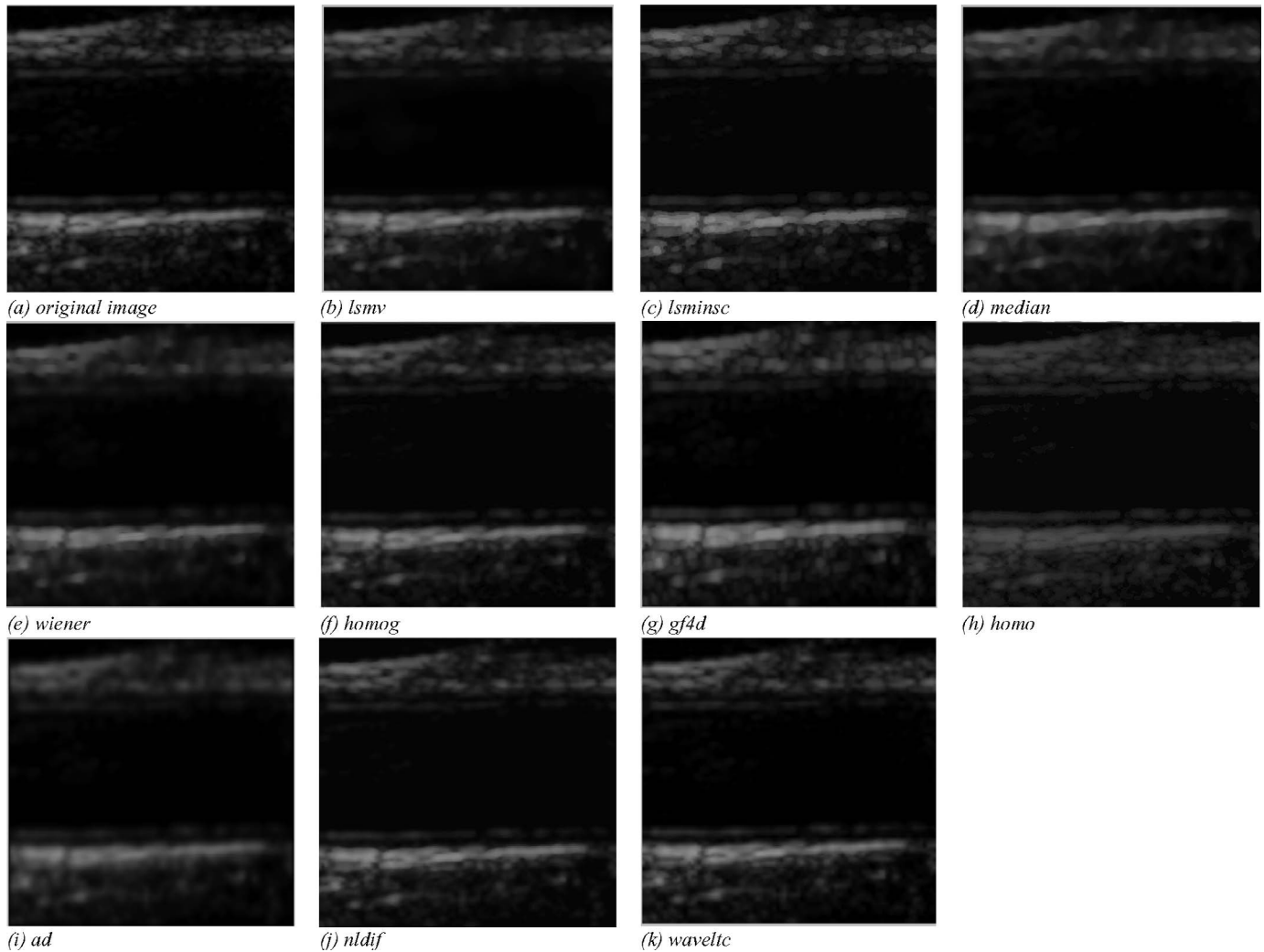


Fig. 2. Original ultrasound image of the carotid artery (2–3 cm proximal to bifurcation) given in (a), and the despeckled filtered images given in (b)–(k).

contrast, correlation, sum of squares variance (SOSV), and sum variance, $\sum Var$. These features were mostly affected after despeckle filtering, and they were significantly different.

D. Texture Analysis: *k*NN Classifier

Table IV shows the percentage of correct classifications score for the *k*NN classifier with $k = 7$ for classifying a subject as asymptomatic or symptomatic. The classifier was evaluated using the leave-one-out method [42], on 220 asymptomatic and 220 symptomatic images on the original and despeckled images. The percentage of correct classifications score is given for the following feature sets: SF, SGLDMm, SGLDMr, GLDS, NGTDM, SFM, Laws TEM, FDTA, and FPS. Filters that showed an improvement in classifications success score compared to that of the original image set were in average (last row of Table IV) the filters homo (3%), gf4d (1%), and lsminsc (1%).

Feature sets that benefited most by the despeckle filtering were the SF, GLDS, NGTDM, and TEM when counting the number of cases that the correct classifica-

tions score was improved. Less improvement was observed for the feature sets FDTA, SFM, SGLDMm, FPS, and SGLDMr. For the feature set SGLDMr better results are given for the lsminsc filter with an improvement of 2%. This is the only filter that showed an improvement for this class of features. For the feature set TEM the filter lsmv shows the best improvement with 9%. For the FPS feature set, the filter lsminsc gave the best improvement with 5%. The filter lsminsc showed improvement in the GLDS and NGTDM feature sets. The filter lsmv showed improvement for the feature sets SF and TEM.

E. Image Quality Evaluation Metrics

Table V tabulates the image quality evaluation metrics presented in Section III-H, for the 220 asymptomatic and 220 symptomatic ultrasound images between the original and the despeckled images, respectively. Best values were obtained for the nldif, lsmv and waveltc with lower MSE, RMSE, Err3, and Err4 and higher SNR and PSNR. The GAE was 0.00 for all cases; this can be attributed to the fact that the information between the original and the de-

TABLE IV
PERCENTAGE OF CORRECT CLASSIFICATIONS SCORE FOR THE kNN CLASSIFIER WITH $k = 7$ FOR THE ORIGINAL AND THE FILTERED IMAGE SETS.¹

| Feature set | No. of feat. | Original | Local statistics | | | Median | HF | GF | HM | Diffusion | | Wavelet |
|-------------|--------------|----------|------------------|-----------|-----------|-----------|-----------|-----------|-----------|-----------|-----------|-----------|
| | | | lsmv | lsmisc | wiener | median | homog | gf4d | homo | ad | nldif | waveltc |
| SF | 5 | 59 | 62 | 61 | 61 | 57 | 63 | 59 | 65 | 60 | 52 | 61 |
| SGLDMm | 13 | 65 | 63 | 64 | 62 | 63 | 69 | 67 | 68 | 61 | 66 | 63 |
| SGLDMr | 13 | 70 | 66 | 72 | 64 | 66 | 65 | 70 | 69 | 64 | 65 | 65 |
| GLDS | 4 | 64 | 63 | 66 | 61 | 69 | 64 | 66 | 72 | 59 | 58 | 62 |
| NGTDM | 5 | 64 | 63 | 68 | 60 | 69 | 63 | 65 | 57 | 60 | 61 | 62 |
| SFM | 4 | 62 | 62 | 60 | 62 | 58 | 55 | 65 | 68 | 59 | 56 | 55 |
| TEM | 6 | 59 | 68 | 52 | 60 | 59 | 66 | 60 | 65 | 53 | 60 | 60 |
| FDTA | 4 | 64 | 63 | 66 | 53 | 68 | 53 | 62 | 73 | 55 | 54 | 62 |
| FPS | 2 | 59 | 54 | 64 | 59 | 58 | 59 | 59 | 59 | 52 | 48 | 55 |
| Average | | 63 | 63 | 64 | 60 | 63 | 62 | 64 | 66 | 58 | 58 | 61 |

¹Bold numbers indicate improvement after despeckling.

²SF, statistical features; SGLDMm, spatial gray level dependence matrix mean values; SGLDMr, spatial gray level dependence matrix range of values; GLDS, gray level difference statistics; NGTDM, neighborhood gray tone difference matrix; SFM, statistical feature matrix; TEM, laws texture energy measures; FDTA, fractal dimension texture analysis; FPS, Fourier power spectrum; HF, homogeneity; GF, geometric; HM, homomorphic.

TABLE V
IMAGE QUALITY EVALUATION METRICS COMPUTED FOR THE 220 ASYMPTOMATIC AND 220 SYMPTOMATIC IMAGES.

| Feature set | Local statistics | | | Median | HF | GF | HM | Diffusion | | Wavelet |
|---------------------|------------------|--------|--------|--------|-------|------|------|-----------|-------|---------|
| | lsmv | lsmisc | wiener | median | homog | gf4d | homo | ad | nldif | waveltc |
| Asymptomatic images | | | | | | | | | | |
| MSE ¹ | 13 | 86 | 19 | 131 | 42 | 182 | 758 | 132 | 8 | 11 |
| RMSE | 3 | 9 | 4 | 10 | 6 | 13 | 27 | 11 | 2 | 3 |
| Err3 | 7 | 17 | 5 | 25 | 14 | 25 | 38 | 21 | 5 | 4 |
| Err4 | 11 | 26 | 7 | 41 | 24 | 40 | 49 | 32 | 10 | 5 |
| GAE | 0 | 0 | 0 | 0 | 0 | 0 | 0 | 0 | 0 | 0 |
| SNR | 25 | 17 | 23 | 16 | 21 | 14 | 5 | 14 | 28 | 25 |
| PSNR | 39 | 29 | 36 | 29 | 34 | 27 | 20 | 28 | 41 | 39 |
| Q | 0.83 | 0.78 | 0.74 | 0.84 | 0.92 | 0.77 | 0.28 | 0.68 | 0.93 | 0.65 |
| SSIN | 0.97 | 0.88 | 0.92 | 0.94 | 0.97 | 0.88 | 0.43 | 0.87 | 0.97 | 0.9 |
| Symptomatic images | | | | | | | | | | |
| MSE | 33 | 374 | 44 | 169 | 110 | 557 | 1452 | 374 | 8 | 23 |
| RMSE | 5 | 19 | 6 | 13 | 10 | 23 | 37 | 19 | 3 | 5 |
| Err3 | 10 | 33 | 9 | 25 | 20 | 43 | 51 | 31 | 5 | 6 |
| Err4 | 16 | 47 | 11 | 38 | 30 | 63 | 64 | 43 | 7 | 8 |
| GAE | 0 | 0 | 0 | 0 | 0 | 0 | 0 | 0 | 0 | 0 |
| SNR | 24 | 13 | 22 | 16 | 17 | 12 | 5 | 12 | 29 | 25 |
| PSNR | 34 | 23 | 33 | 26 | 28 | 21 | 17 | 23 | 39 | 36 |
| Q | 0.82 | 0.77 | 0.7 | 0.79 | 0.87 | 0.75 | 0.24 | 0.63 | 0.87 | 0.49 |
| SSIN | 0.97 | 0.85 | 0.89 | 0.81 | 0.94 | 0.85 | 0.28 | 0.81 | 0.97 | 0.87 |

¹MSE, mean square error; RMSE, randomized mean square error; Err3, Err4, Minowski metrics; GAE, geometric average error; SNR, signal-to-noise ratio; PSNR, peak signal-to-noise ratio; Q, universal quality index; SSIN, structural similarity index.

speckled images remains unchanged. Best values for the universal quality index, Q , and the structural similarity index, SSIN were obtained for the filters lsmv and nldif.

F. Visual Evaluation by Experts

Table VI shows the results of the visual evaluation of the original and despeckled images made by two experts, a cardiovascular surgeon and a neurovascular specialist. The

last row of Table VI presents the overall average percentage (%) score assigned by both experts for each filter.

For the cardiovascular surgeon, the average score showed that the best despeckle filter is the lsmv with a score of 62%, followed by gf4d, median, homog and original with scores of 52%, 50%, 45%, and 41%, respectively. For the neurovascular specialist, the average score showed that the best filter is the gf4d with a score of 72%, followed by lsmv, original, lsmisc and median with scores of

TABLE VI
 PERCENTAGE SCORING OF VISUAL EVALUATION OF THE ORIGINAL AND DESPECKLED IMAGES [50 ASYMPTOMATIC (A) AND 50 SYMPTOMATIC (S)] BY THE EXPERTS.

| Experts | A/S | Local statistics | | | Median | HF ¹ | GF | HM | Diffusion | Wavelet |
|--------------------------|-----|------------------|------|--------|--------|-----------------|------|------|-----------|---------|
| | | Original | lsmv | lsmnsc | median | homog | gf4d | homo | nldif | waveltc |
| Cardiovascular Surgeon | A | 33 | 75 | 33 | 43 | 47 | 61 | 19 | 43 | 32 |
| Average % | S | 48 | 49 | 18 | 57 | 43 | 42 | 20 | 33 | 22 |
| Neurovascular Specialist | A | 41 | 62 | 26 | 50 | 45 | 52 | 19 | 38 | 27 |
| Average % | S | 70 | 76 | 73 | 74 | 63 | 79 | 23 | 52 | 29 |
| Overall average % | | 66 | 67 | 63 | 58 | 45 | 65 | 55 | 41 | 28 |
| | | 68 | 71 | 68 | 66 | 54 | 72 | 39 | 47 | 28 |
| | | 54 | 67 | 47 | 58 | 50 | 62 | 29 | 43 | 28 |

¹HF, homogeneity; GF, geometric; HM, homomorphic.

71%, 68%, 68%, and 66%, respectively. The overall average percent score shows that the highest score was given to the filter lsmv (67%), followed by gf4d (62%), median (58%), and original (54%). It should be emphasized that the despeckle filter lsmv is the only filter that was graded with a higher score than the original by both experts for the asymptomatic and symptomatic image sets.

We may observe a difference in the scorings between the two vascular specialists. This is because the cardiovascular surgeon is primarily interested in the plaque composition and texture evaluation, and the neurovascular specialist is interested in evaluating the degree of stenosis and the lumen diameter in order to identify the plaque contour. Filters lsmv and gf4d were identified as the best despeckle filters by both specialists as they improved visual perception with overall average scores of 67% and 62%, respectively. The filters waveltc and homo were scored by both specialists with the lowest overall average scores of 28% and 29%, respectively.

By examining the visual results of Fig. 2, the statistical results of Tables II–V and the visual evaluation of Table VI, we can conclude that the best filters are lsmv and gf4d, which may be used for both plaque composition enhancement and plaque texture analysis. The filters lsmv, gf4d, and lsmnsc are more appropriate to identify the degree of stenosis and, therefore, may be used when the primary interest is to outline the plaque borders.

V. DISCUSSION

Despeckle filtering is an important operation in the enhancement of ultrasound images of the carotid artery, in both the case of texture analysis, image quality evaluation, and visual evaluation by the experts. In this study, a total of 10 despeckle filters were comparatively evaluated on 440 ultrasound images of the carotid artery bifurcation, and the validation results are summarized in Table VII.

As given in Table VII, filters lsmv, lsmnsc, and homo, improved the class separation between the asymptomatic and the symptomatic classes (see also Table II). Filters lsmv, lsmnsc, and gf4d gave a high number of significantly different features (see Table III). Filters lsmnsc, gf4d, and homo gave only a marginal improvement in the percent-

age of correct classifications success rate (see Table IV). Moreover, filters lsmv, nldif, and waveltc gave better image quality evaluation results (see Table V). Filters lsmv and gf4d improved the visual assessment carried out by the experts (see Table VI). It is clearly shown that filter lsmv gave the best performance, followed by filters lsmnsc and gf4d (see Table VII). Filters lsmv or gf4d can be used for despeckling asymptomatic images in which the expert is interested mainly in the plaque composition and texture analysis. Filters lsmv, gf4d, or lsmnsc can be used for despeckling of symptomatic images in which the expert is interested in identifying the degree of stenosis and the plaque borders. Filters homo, nldif, and waveltc gave poorer performance.

Filter lsmv gave very good performance with respect to: preserving the mean and the median as well as decreasing the variance and the speckle index of the image; increasing the distance of the texture features between the asymptomatic and the symptomatic classes; significantly changing the SGLDM range of values texture features after filtering based on the Wilcoxon rank sum test; marginally improving the classification success rate of the kNN classifier for the classification of asymptomatic and symptomatic images in the cases of SF, SMF, and TEM feature sets; and improving the image quality of the image. The lsmv filter, which is a simple filter, is based on local image statistics. It was first introduced in [9], [14], [15] by Lee, and it was tested on a few SAR images with satisfactory results. It also was used for SAR imaging in [13] and image restoration in [16], again with satisfactory results.

Filter lsmnsc gave the best performance with respect to: preserving the mean, as well as decreasing the variance and the speckle index and increasing the contrast of the image; increasing the distance of the texture features between the asymptomatic and the symptomatic classes; significantly changing the SGLDM texture features after filtering based on the Wilcoxon rank sum test; improving the classification success rate of the kNN classifier for the classification of asymptomatic and symptomatic images in the cases of SF, SGLDMr, GLDS, NGTDM, FDTA, and FPS feature sets. Filter lsmnsc was originally introduced by Nagao and Matsuyama in [32] and was tested on an

TABLE VII
SUMMARY FINDINGS OF DESPECKLE FILTERING IN ULTRASOUND IMAGING OF THE CAROTID ARTERY.

| Despeckle filter | Statistical and texture features Table II | Statistical analysis Table III | kNN classifier Table IV | Image quality evaluation Table V | Optical perception evaluation Table VI |
|-----------------------|--|-----------------------------------|----------------------------|-------------------------------------|---|
| Local statistics | | | | | |
| lsmv | ✓ | ✓ | | ✓ | ✓ |
| lsmisc | ✓ | ✓ | ✓ | | |
| Geometric filtering | | | | | |
| gf4d | | ✓ | ✓ | | ✓ |
| Homomorphic filtering | | | | | |
| homo | ✓ | | ✓ | | |
| Diffusion filtering | | | | | |
| nldif | | | | ✓ | |
| Wavelet filtering | | | | | |
| waveltc | | | | ✓ | |

artificial and a SAR image with satisfactory performance. In this study the filter was modified, by using the speckle index instead of the variance value for each subwindow [as described in Section II-A,2, (9)].

Filter gf4d gave very good performance with respect to: decreasing the speckle index; marginally increasing the distance of the texture features between the asymptomatic and the symptomatic classes; significantly changing the SGLDM range of values texture features after filtering based on the Wilcoxon rank sum test; improving the classification success rate of the kNN classifier for the classification of asymptomatic and symptomatic images in the cases of SGLDMm, GLDS, NGTDM, SFM, and TEM feature sets. The geometric filter gf4d was introduced by Busse *et al.* [10] and was tested visually on a few SAR images with satisfactory results.

Filters used for speckle reduction in ultrasound imaging by other investigators include: median [33], wiener [13], homog [8], homo [17], [18], ad [5], and waveltc [29]. However, these filters were evaluated on a small number of images, and their performance was tested based only on the mean, median, standard deviation, and speckle index of the image before and after filtering.

The median and the wiener filters were originally used by many researchers for suppressing the additive and later for suppressing the multiplicative noise in different types of images [2]–[9], [13], [33]. The results of this study showed that the wiener and median filters were not able to remove the speckle noise and produced blurred edges in the filtered image (see Fig. 2). In this study the median filter performed poorer as shown in Tables II and III, and IV.

The homog [8] and homo [2], [17], [18] filters, were recently used by some researchers for speckle reduction, but our results in Tables II, III, and V and the visual evaluation of the experts in Table VI showed poor performance, especially for the homo filter.

Anisotropic diffusion is an efficient, nonlinear technique for simultaneously performing contrast enhancement and noise reduction. It smoothes homogeneous image regions but retains image edges [23]. Anisotropic diffusion filters

usually require many iteration steps compared with the local statistic filters. In a recent study [5], speckle-reducing anisotropic diffusion filtering was proposed as the most appropriate filter for ultrasound images of the carotid artery. However, in this study, ad, as shown in Tables II, III, IV, V, and VI, performed poorer compared to lsmv, gf4d, and lsmisc.

Furthermore, wavelet filtering proposed by Donoho [29] was investigated for suppressing the speckle noise in SAR images [15], [35], real world images [25], and ultrasound images [26] with favorable results. In this study, it is shown that the waveltc filter gave poorer performance for removing the speckle noise from the ultrasound images of the carotid artery (Tables II, III).

VI. CONCLUSION

Despeckle filtering is an important operation in the enhancement of ultrasonic imaging of the carotid artery. In this study it was shown that simple filters based on local statistics (lsmv and lsmisc) and geometric filtering (gf4d) could be used successfully for the processing of these images. In this context, despeckle filtering can be used as a preprocessing step for the automated segmentation of the IMT [52] and the carotid plaque, followed by the carotid plaque texture analysis, and classification. This field is currently being investigated by our group [53]. Initial findings show promising results; however, further work is required to evaluate the performance of the suggested despeckle filters at a larger scale as well as their impact in clinical practice. In addition, the usefulness of the proposed despeckle filters in portable ultrasound systems and in wireless telemedicine systems still has to be investigated.

ACKNOWLEDGMENTS

This work was partly funded through the project Integrated System for the Support of the Diagnosis for the Risk of Stroke (IASIS), of the 5th Annual Program for the

Financing of Research of the Research Promotion Foundation of Cyprus 2002–2005, as well as through the project Integrated System for the Evaluation of Ultrasound Imaging of the Carotid Artery (TALOS), of the Program for Research and Technological Development 2003–2005, of the Research Promotion Foundation of Cyprus.

REFERENCES

- [1] D. Lamont, L. Parker, M. White, N. Unwin, S. M. A. Bennett, M. Cohen, D. Richardson, H. O. Dickinson, A. Adamson, K. G. M. M. Alberti, and A. W. Graft, "Risk of cardiovascular disease measured by carotid intima-media thickness at age 49–51: Life course study," *Brit. Med. J.*, vol. 320, pp. 273–278, Jan. 29, 2000.
- [2] C. B. Burckhardt, "Speckle in ultrasound B-mode scans," *IEEE Trans. Sonics Ultrason.*, vol. SU-25, no. 1, pp. 1–6, 1978.
- [3] R. F. Wagner, S. W. Smith, J. M. Sandrik, and H. Lopez, "Statistics of speckle in ultrasound B-scans," *IEEE Trans. Sonics Ultrason.*, vol. 30, pp. 156–163, 1983.
- [4] J. W. Goodman, "Some fundamental properties of speckle," *J. Opt. Soc. Amer.*, vol. 66, no. 11, pp. 1145–1149, 1976.
- [5] Y. Yongjian and S. T. Acton, "Speckle reducing anisotropic diffusion," *IEEE Trans. Image Processing*, vol. 11, no. 11, pp. 1260–1270, Nov. 2002.
- [6] R. W. Prager, A. H. Gee, G. M. Treece, and L. Berman, "Speckle detection in ultrasound images using first order statistics," *GUED/F-INFENG/TR*, University of Cambridge, Department of Engineering, Internal Report, vol. 415, pp. 1–17, Jul. 2002.
- [7] C. Loizou, C. Christodoulou, C. S. Pattichis, R. Istepanian, M. Pantziaris, and A. Nicolaides, "Speckle reduction in ultrasound images of atherosclerotic carotid plaque," in *Proc. IEEE 14th Int. Conf. Digital Signal Processing*, vol. 2, July 2002, pp. 525–528.
- [8] C. I. Christodoulou, C. Loizou, C. S. Pattichis, M. Pantziaris, E. Kyriakou, M. S. Pattichis, C. N. Schizas, and A. Nicolaides, "Despeckle filtering in ultrasound imaging of the carotid artery," in *Proc. Second Joint Eng. Med. Biol./Biomed. Eng. Soc. (EMBS/BMES)*, 2002, pp. 1027–1028.
- [9] J. S. Lee, "Speckle analysis and smoothing of synthetic aperture radar images," *Comput. Graph. Image Processing*, vol. 17, pp. 24–32, 1981.
- [10] L. Busse, T. R. Crimmins, and J. R. Fienup, "A model based approach to improve the performance of the geometric filtering speckle reduction algorithm," in *Proc. IEEE Ultrason. Symp.*, 1995, pp. 1353–1356.
- [11] D. T. Kuan, A. A. Sawchuk, T. C. Strand, and P. Chavel, "Adaptive restoration of images with speckle," *IEEE Trans. Acoust. Speech Signal Processing*, vol. ASSP-35, pp. 373–383, 1987.
- [12] M. Insana, T. J. Hall, G. G. Cox, and J. S. Rosenthal, "Progress in quantitative ultrasonic imaging," in *Proc. SPIE Medical Imaging III, Image Formation*, vol. 1090, pp. 2–9, 1989.
- [13] V. S. Frost, J. A. Stiles, K. S. Shanmuggam, and J. C. Holtzman, "A model for radar images and its application for adaptive digital filtering of multiplicative noise," *IEEE Trans. Pattern Anal. Machine Intell.*, vol. 4, no. 2, pp. 157–165, 1982.
- [14] J. S. Lee, "Digital image enhancement and noise filtering by using local statistics," *IEEE Trans. Pattern Anal. Machine Intell.*, vol. PAMI-2, no. 2, pp. 165–168, 1980.
- [15] J. S. Lee, "Refined filtering of image noise using local statistics," *Comput. Graph. Image Processing*, vol. 15, pp. 380–389, 1981.
- [16] D. T. Kuan and A. A. Sawchuk, "Adaptive noise smoothing filter for images with signal dependent noise," *IEEE Trans. Pattern Anal. Machine Intell.*, vol. PAMI-7, no. 2, pp. 165–177, 1985.
- [17] S. Solbo and T. Eltoft, "Homomorphic wavelet based-statistical despeckling of SAR images," *IEEE Trans. Geosc. Remote Sensing*, vol. 42, no. 4, pp. 711–721, 2004.
- [18] J. Saniie, T. Wang, and N. Bilgutay, "Analysis of homomorphic processing for ultrasonic grain signal characterization," *IEEE Trans. Ultrason., Ferroelect., Freq. Contr.*, vol. 3, pp. 365–375, 1989.
- [19] S. Jin, Y. Wang, and J. Hiller, "An adaptive non-linear diffusion algorithm for filtering medical images," *IEEE Trans. Inform. Technol. Biomed.*, vol. 4, no. 4, pp. 298–305, Dec. 2000.
- [20] J. Weickert, B. Romery, and M. Viergever, "Efficient and reliable schemes for nonlinear diffusion filtering," *IEEE Trans. Image Processing*, vol. 7, pp. 398–410, 1998.
- [21] N. Rougon and F. Preteux, "Controlled anisotropic diffusion," in *Proc. SPIE Conf. Nonlinear Image Processing VI, IS&T/SPIE*, San Jose, CA, vol. 2424, 1995, pp. 329–340.
- [22] M. Black, G. Sapiro, D. Marimont, and D. Heeger, "Robust anisotropic diffusion," *IEEE Trans. Image Processing*, vol. 7, no. 3, pp. 421–432, Mar. 1998.
- [23] P. Rerona and J. Malik, "Scale-space and edge detection using anisotropic diffusion," *IEEE Trans. Pattern Anal. Machine Intell.*, vol. 12, no. 7, pp. 629–639, July 1990.
- [24] K. Abd-Elmoniem, A.-B. Youssef, and Y. Kadah, "Real-time speckle reduction and coherence enhancement in ultrasound imaging via nonlinear anisotropic diffusion," *IEEE Trans. Biomed. Eng.*, vol. 49, no. 9, pp. 997–1014, Sep. 2002.
- [25] S. Zhong and V. Cherkassky, "Image denoising using wavelet thresholding and model selection," in *Proc. IEEE Int. Conf. Image Processing*, Nov. 2000, pp. 1–4.
- [26] A. Achim, A. Bezerianos, and P. Tsakalides, "Novel Bayesian multiscale method for speckle removal in medical ultrasound images," *IEEE Trans. Med. Imag.*, vol. 20, no. 8, pp. 772–783, 2001.
- [27] X. Zong, A. Laine, and E. Geiser, "Speckle reduction and contrast enhancement of echocardiograms via multiscale nonlinear processing," *IEEE Trans. Med. Imag.*, vol. 17, no. 4, pp. 532–540, 1998.
- [28] X. Hao, S. Gao, and X. Gao, "A novel multiscale nonlinear thresholding method for ultrasonic speckle suppressing," *IEEE Trans. Med. Imag.*, vol. 18, no. 9, pp. 787–794, 1999.
- [29] D. L. Donoho, "Denoising by soft thresholding," *IEEE Trans. Inform. Theory*, vol. 41, pp. 613–627, 1995.
- [30] A. M. Wink and J. B. T. M. Roerdink, "Denoising functional MR images: A comparison of wavelet denoising and Gaussian smoothing," *IEEE Trans. Med. Imag.*, vol. 23, no. 3, pp. 374–387, 2004.
- [31] V. Dutt, "Statistical analysis of ultrasound echo envelope," Ph.D. dissertation, Mayo Graduate School, Rochester, MN, 1995.
- [32] M. Nagao and T. Matsuyama, "Edge preserving smoothing," *Comput. Graph. Image Processing*, vol. 9, pp. 394–407, 1979.
- [33] T. Huang, G. Yang, and G. Tang, "A fast two-dimensional median filtering algorithm," *IEEE Trans. Acoust. Speech Signal Processing*, vol. 27, no. 1, pp. 13–18, 1979.
- [34] S. M. Ali and R. E. Burge, "New automatic techniques for smoothing and segmenting SAR images," *Signal Processing*, vol. 14, pp. 335–346, 1988.
- [35] F. N. S. Medeiros, N. D. A. Mascarenhas, R. C. P. Marques, and C. M. Laprano, "Edge preserving wavelet speckle filtering," in *Proc. 5th IEEE Southwest Symp. Image Anal. Interpretation*, April 7–9, 2002, pp. 281–285.
- [36] S. Gupta, R. C. Chauhan, and S. C. Sexana, "Wavelet-based statistical approach for speckle reduction in medical ultrasound images," *Med. Biol. Eng. Comput.*, vol. 42, pp. 189–192, 2004.
- [37] "Comparison of image clarity, SonoCT real-time compound imaging versus conventional 2D ultrasound imaging," Bothell, WA: ATL Ultrasound, Report no. G55203r1, 2001.
- [38] C. Christodoulou, C. Pattichis, M. Pantziaris, and A. Nicolaides, "Texture-based classification of atherosclerotic carotid plaques," *IEEE Trans. Med. Imag.*, vol. 22, no. 7, pp. 902–912, 2003.
- [39] R. M. Haralick, K. Shanmuggam, and I. Dinstein, "Texture features for image classification," *IEEE Trans. Syst., Man. Cybern.*, vol. SMC-3, pp. 610–621, Nov. 1973.
- [40] J. S. Weszka, C. R. Dyer, and A. Rosenfield, "A comparative study of texture measures for terrain classification," *IEEE Trans. Syst., Man. Cybern.*, vol. SMC-6, pp. 269–285, Apr. 1976.
- [41] M. Amadasun and R. King, "Textural features corresponding to textural properties," *IEEE Trans. Syst., Man. Cybern.*, vol. 19, no. 5, pp. 1264–1274, Sep. 1989.
- [42] C. M. Wu, Y. C. Chen, and K.-S. Hsieh, "Texture features for classification of ultrasonic images," *IEEE Trans. Med. Imag.*, vol. 11, pp. 141–152, June 1992.

- [43] T. J. Chen, K. S. Chuang, J. Wu, S. C. Chen, I. M. Hwang, and M. L. Jan, "A novel image quality index using Moran I statistics," *Phys. Med. Biol.*, vol. 48, pp. 131–137, 2003.
- [44] R. Gonzalez and R. Woods, *Digital Image Processing*. 2nd ed. Upper Saddle River, NJ: Prentice-Hall, 2002, pp. 419–420.
- [45] Z. Wang, A. Bovik, H. Sheikh, and E. Simoncelli, "Image quality assessment: From error measurement to structural similarity," *IEEE Trans. Image Processing*, vol. 13, no. 4, pp. 600–612, Apr. 2004.
- [46] S. Winkler, "Vision models and quality metrics for image processing applications," Ph.D. dissertation, University of Lausanne-Switzerland, Dec. 21, 2000.
- [47] D. Sakrison, "On the role of observer and a distortion measure in image transmission," *IEEE Trans. Commun.*, vol. 25, pp. 1251–1267, Nov. 1977.
- [48] Z. Wang and A. Bovik, "A universal quality index," *IEEE Signal Processing Lett.*, vol. 9, no. 3, pp. 81–84, Mar. 2002.
- [49] H. R. Sheikh, A. C. Bovik, and G. de Veciana, "An information fidelity criterion for image quality assessment using natural scene statistics," *IEEE Trans. Image Processing*, to be published.
- [50] E. Krupinski, H. Kundel, P. Judy, and C. Nodine, "The medical image perception society: Key issues for image perception research," *Radiology*, vol. 209, pp. 611–612, 1998.
- [51] T. Elatrozy, A. Nicolaides, T. Tegos, A. Zarka, M. Griffin, and M. Sabetai, "The effect of B-mode ultrasonic image standardization of the echodensity of symptomatic and asymptomatic carotid bifurcation plaque," *Int. Angiol.*, vol. 17, no. 3, pp. 179–186, Sep. 1998.
- [52] C. Loizou, C. Pattichis, R. Istepanian, and M. Pantziaris, "Intima media segmentation of the carotid artery," in *Proc. Medicon X Mediterranean Conf. Med. Biol. Eng., Health Inform. Soc.*, July 31–August 5, 2004.
- [53] C. S. Pattichis, E. Kyriakou, C. Christodoulou, M. S. Pattichis, C. Loizou, M. Pantziaris, and A. Nicolaides, "Cardiovascular: Ultrasound imaging in vascular cases," in *Wiley Encyclopaedia of Biomedical Engineering*. M. Akay, Ed. New York: Wiley, 2006, to be published.



Christos P. Loizou obtained his first degree (B.Sc.) in Germany at the University of Kaiserslautern, Kaiserslautern, Germany, in electrical engineering in 1986, then had a master's specialization in telecommunications obtaining a Dipl.-Ing. degree (M.Sc.) at the same university in 1990. He had his final thesis in medical image processing. He has a specialization in medical image processing.

From 1990 to 1996 he was involved with research in medical image processing. From 1996 to 2000 he was a lecturer at Higher Technical

Institute in Nicosia, Cyprus, teaching in the Computer Science Department. Since 2000 he is senior lecturer at Intercollege Limassol Campus, Limassol, Cyprus, teaching computer science courses at the B.Sc. and M.Sc. levels. He is pursuing his Ph.D. degree research in the area of ultrasound image of the carotid artery at Kingston University, London, UK, in collaboration with the Institute of Neurology and Genetics in Nicosia, Cyprus.

His research interests include medical imaging, signal and image processing, pattern recognition, biosignal analysis, and computer applications in medicine.



Constantinos S. Pattichis (S'88–M'88–SM'99) received his diploma as a technician engineer from the Higher Technical Institute in Nicosia, Cyprus, the B.Sc. degree in electrical engineering from the University of New Brunswick, Fredericton, Canada, the M.Sc. degree in biomedical engineering from the University of Texas, Austin, the M.Sc. degree in neurology from the University of Newcastle Upon Tyne, Newcastle, UK, and the Ph.D. degree in electronic engineering from the University of London, London, UK.

He is an associate professor with the Department of Computer Science of the University of Cyprus, Nicosia, Cyprus, and a senior scientist of the Department of Computational Intelligence of the Cyprus Institute of Neurology and Genetics, Nicosia, Cyprus. His current research interests include health telematics, medical imaging, biosignal analysis, and computational intelligence systems in medicine and in bioinformatics.

He has published 15 chapters in books, 33 refereed journal articles, and 95 conference papers in these areas. He is co-editor of the forthcoming book *M-Health: Emerging Mobile Health Systems*, to be published by Springer Science in 2005. He was guest co-editor of the Special Issue on Emerging Health Telematics Applications in Europe of the *IEEE Transactions on Information Technology in Biomedicine*, and Chairman of the Medical and Biological Engineering and Computing Conference 98, and the IEEE Melecon 2000. He served as chairman of the IEEE Cyprus Section, and the Cyprus Society of Biomedical Engineering and Medical Physics. He serves as associate editor of the *IEEE Transactions on Information Technology in Biomedicine* and *IEEE Transactions on Neural Networks* and is a senior member of the IEEE.



Christodoulos I. Christodoulou studied electrical engineering with specialization in telecommunications at the Technical University in Aachen, Germany, where he graduated in 1987. He received the Ph.D. degree in electronics engineering from the Queen Mary University, London, in 2000. He carries out his research work in cooperation with the Computational Intelligence Department of the Cyprus Institute of Neurology and Genetics, Nicosia, Cyprus, and with the Department of Computer Science of the University

of Cyprus in Nicosia, Cyprus.

His research interests include intelligent information systems, artificial neural networks, signal and image processing, pattern recognition, biosignal analysis, and computer applications in medicine.



Robert S. H. Istepanian obtained his Ph.D. degree from the Electronic and Electrical Engineering Department, Loughborough University, Loughborough, Leicestershire, UK, in 1994. From 1984 to 1998 he worked in different overseas industrial and academic positions. In 1988 he was a visiting Research Fellow in the Department of Electronic and Electrical Engineering, Loughborough University, UK. He was with the same department from 1994–1995 as a postdoctoral Research Fellow. From 1996 to 1999 he was a

senior lecturer at the University of Portsmouth, Portsmouth, UK. From 1999–2000, he was an associate professor at the Universities of Western Ontario and Ryerson in Toronto, ON, Canada. From 2000 to 2003, he was a senior lecturer and head of the Mobile Information Engineering and E-Med Systems research group in the Department of Electronic and Computer Engineering Brunel University, West London, UK.

In 2003, he joined the School of Computing and Information Systems, Kingston University, London, UK, as a professor of data communications and Director of Mobile Information and Network Technologies (MINT) Research Centre in the University.

Dr. Istepanian is a Fellow of the Institute of Electrical Engineers and a Senior Member of the IEEE. He currently serves on the editorial boards of the *IEEE Transaction on Information Technology in Biomedicine* and was one of the founding special area editors of the *IEEE Transaction on Information Technology in Biomedicine* and telemedicine and e-health since 1997. He has served as guest editor of three special issues of the *IEEE Transactions on Information Technology in Biomedicine* and the *IEEE Transaction on NanoBioScience* since 1999. He is also an associate editor of the *Journal*

of *Mobile Multimedia* and *Journal on Information Technology in Healthcare*.

He has published more than 140-refereed journal and conference papers and three books, including chapters in these books in the areas of biomedical signals processing and mobile communications for healthcare and m-health technologies.



Marios Pantziaris received his M.D. in neurology in 1995 in Thessaloniki, Greece. He has been trained in Carotid Duplex—Doppler ultrasonography in London at St. Mary's Hospital in 1995, and in 1999 he followed training as a visiting doctor in acute stroke treatment in Massachusetts General Hospital, Harvard University, Boston.

He is working at the Cyprus Institute of Neurology and Genetics, Nicosia, Cyprus, as a senior neurologist in the Neurological Department and he is the Head of the Neurovascular Department. He has considerable experience in carotids—transcranial ultrasound, and he has participated in many research projects and publications in that area.

Dr. Pantziaris is also Head of the Multiple Sclerosis (MS) clinic where he is running research projects towards the aetiology and therapy of MS. He has given many lectures about MS, carotids ultrasound, and stroke in Cyprus and abroad.



Andrew Nicolaides is a graduate of the Pancyprian Gymnasium, Nicosia, Cyprus, and Guy's Hospital Medical School, London University, 1962, and a Fellow of the Royal College of Surgeons England, and the Royal College of Surgeons Edinburgh (1967).

His higher surgical training was in Oxford University, Kings College Hospital Medical School, London, UK, and St. Mary's Hospital Medical School, London. He was awarded the Jacksonian prize by the Royal College of Surgeons England in 1972 for his work on the

prevention of venous thromboembolism and obtained the degree of M.S. (Master of Surgery) in 1976.

He was the Professor of Vascular Surgery at the Imperial College School of Medicine, St. Mary's Hospital, and Consultant Vascular Surgeon at St. Mary's Hospital from 1983–2000 and Medical Director of the Cyprus Institute of Neurology and Genetics, Nicosia, Cyprus, from 2001–2004. His research group is known internationally in several areas which include noninvasive vascular screening and diagnostic investigation, early detection and prevention of cardiovascular and venous disease. His research is now directed toward the genetic risk factors for cardiovascular disease, identification of individuals at risk, and the development of effective methods of prevention, especially stroke. He is past-president of the International Union of Angiology and past-president of the Section of Measurement in Medicine of the Royal Society of Medicine.

Dr. Nicolaides has received many awards and honorary memberships from many scientific societies. He is Editor-in-Chief of *International Angiology* and is on the Editorial Board of many vascular journals. He is Professor Emeritus at Imperial College, London, UK, and an examiner for M.S. and Ph.D. degrees for London University. He is a "Special Scientist" at the University of Cyprus, Nicosia, Cyprus, and Medical Director of the Vascular Screening and Diagnostic Centre in London. He has trained over 200 vascular surgeons who are practicing all over the world; 10 of them are holding prestigious Chairs as professors in vascular surgery. He was made Archon Megas Referendarios, an Honour bestowed by the Patriarch of Constantinople in 1994. He is co-author of over 400 original papers and editor of 14 books.